Journal of Solid State Chemistry 183 (2010) 1347–1353

Contents lists available at ScienceDirect

Journal of Solid State Chemistry

journal homepage: www.elsevier.com/locate/jssc

Synthesis and characterization of $La_{1+x}Sr_{2-x}CoMnO_{7-\delta}$ ($x=0,0.2$; $\delta=0,1$)

H. El Shinawi [a], A. Bertha [b], J. Hadermann [b], T. Herranz [c], B. Santos [c], J.F. Marco [c], F.J. Berry [a], C. Greaves [a,*]

[a] School of Chemistry, University of Birmingham, Birmingham B15 2TT, UK
[b] EMAT, RUCA, Groenenborgerlaan 171, Antwerp 2020, Belgium
[c] Instituto de Quimica-Fisica "Rocasolano", Serrano 119, CSIC, 28006 Madrid, Spain

ARTICLE INFO

Article history:
Received 19 February 2010
Received in revised form
8 April 2010
Accepted 13 April 2010
Available online 28 April 2010

Keywords:
Ruddlesden–Popper
$LaSr_2CoMnO_7$
$LaSr_2CoMnO_6$
Neutron diffraction
Spin glass

ABSTRACT

The $n=2$ Ruddlesden–Popper phases $LaSr_2CoMnO_7$ and $La_{1.2}Sr_{1.8}CoMnO_7$ have been synthesized by a sol–gel method. The O6-type phases $LaSr_2CoMnO_6$ and $La_{1.2}Sr_{1.8}CoMnO_6$ were produced by reduction of the O7 phases under a hydrogen atmosphere. The materials crystallize in the tetragonal $I4/mmm$ space group with no evidence of long-range cation order in the neutron and electron diffraction data. Oxygen vacancies in the reduced materials are located primarily at the common apex of the double perovskite layers giving rise to square pyramidal coordination around cobalt and manganese ions. The oxidation states Co^{3+}/Mn^{4+} and Co^{2+}/Mn^{3+} predominate in the as-prepared and reduced materials, respectively. The materials are spin glasses at low temperature and the dominant magnetic interactions change from ferro- to antiferromagnetic following reduction.

1. Introduction

Perovskite-type oxides that exhibit oxygen nonstoichiometry and mixed transition metal valency under various oxygen partial pressure environments are of considerable interest as potential materials for solid oxide fuel cells and oxygen separation membranes. The Ruddlesden Popper (RP) type oxides have shown a special aptitude for oxygen deficiency that alters not only the transition metal oxidation states but also modifies the magnetic and transport properties of these phases. This can be related to the ability of these phases to accommodate a range of metal coordination environments and oxidation states. Oxygen deficiency can be produced in these materials through synthesis in air/inert atmosphere in order to achieve lower oxidation states of the B-site cations (e.g. $Sr_3M_2O_{7-\delta}$, M=Co, Fe [1–5]). Oxygen deficiency can also be induced by controlled reduction of near-stoichiometric phases in hydrogen. Examples include many $n=1$ RP phases such as $La_{2-x}Sr_xNiO_{4-\delta}$ [6,7] and $La_{2-x}Sr_xCo_{0.5}Fe_{0.5}O_{4-\delta}$ [8,9]. Powerful reducing agents such as calcium hydride have recently been used to produce highly oxygen-deficient phases in which unusual two-dimensional coordination geometries of transition metal ions such as cobalt and iron have been achieved [10,11].

In the $n=1$ RP phases, the oxide ion vacancies preferentially distribute within the MO_2 planes of the perovskite layers where the vacancies may be ordered [6,7,12] or disordered [8,9,13]. A disordered distribution of vacancies within the equatorial MO_2 planes has also been reported for the $n=2$ RP $Sr_3Mn_2O_{6.55}$ [14]. The O6 variant of this material ($Sr_3Mn_2O_6$) has been shown by Greaves et al. [15] to exhibit vacancy order within the MO_2 planes. In contrast, the $n=2$ RP phases containing cobalt and iron systematically loose oxygen from the apical sites linking the MO_6 octahedra to provide a square pyramidal coordination around the transition metal ions in the O6 phase [1,2]; this framework was first observed for $La_{2-x}Sr_{1+x}Cu_2O_6$ [16]. Phases with oxygen stoichiometry less than 6 have vacancies located within the MO_2 planes as well as the linking apical sites [3–5]. The synthesis of $LaSr_2CoMnO_7$ by a standard ceramic method has recently been reported [17] and the structural and magnetic properties described. The low temperature magnetic behaviour suggested an additional transition below a spin glass transition. In order to reconsider the magnetic characteristics, $LaSr_2CoMnO_7$ has been re-examined, but prepared here by a sol–gel technique, and compared with $La_{1.2}Sr_{1.8}CoMnO_7$ which has modified cation oxidation states. These two materials have been subsequently reduced in a H_2/N_2 atmosphere to give the O6-like phases. We describe here the synthesis, structural and magnetic characterization of $LaSr_2CoMnO_7$, $La_{1.2}Sr_{1.8}CoMnO_7$, $LaSr_2CoMnO_6$ and $La_{1.2}Sr_{1.8}CoMnO_6$; in the latter reduced phases, the anion vacancies are primarily located in the sites which form the common apex of the double perovskite layers.

* Corresponding author.
E-mail address: c.greaves@bham.ac.uk (C. Greaves).

0022-4596/$ - see front matter © 2010 Elsevier Inc. All rights reserved.
doi:10.1016/j.jssc.2010.04.018

2. Experimental

The materials $LaSr_2CoMnO_7$ and $La_{1.2}Sr_{1.8}CoMnO_7$ were synthesized by a sol–gel procedure using La_2O_3 (previously heated at 800 °C in air for 12 h to remove residual water and carbonate) $SrCO_3$, $Co(CH_3COO)_2 \times 4H_2O$ and $Mn(CH_3COO)_2 \cdot 4H_2O$ as starting materials. Stoichiometric amounts of the starting materials were dissolved in acetic acid and boiled under reflux for 3 h. Small amounts of hydrogen peroxide and water were added and the mixture was further refluxed overnight to obtain a clear solution. This solution was evaporated to a dark violet gel which was then dried and heated in air at 400 °C. The resulting powder was pressed into pellets and calcined in flowing oxygen at 1350 °C for 18 h. The oxygen deficient variants ($LaSr_2CoMnO_6$ and $La_{1.2}Sr_{1.8}CoMnO_6$) were obtained by reducing the as-prepared materials in a mixture of flowing 10% H_2/N_2 for 12 h at 700 °C. X-ray powder diffraction (XRD) data were collected using a Siemens D5000 diffractometer in transmission mode with Cu$K\alpha_1$ radiation from a germanium monochromator. Thermogravimetric analysis (TG) was performed using a Rheometric Scientific STA 1500 thermal analyzer where samples (~30 mg) were reduced at 10 °C/min in 10% H_2/N_2. Neutron powder diffraction (NPD) data were collected at 298 K on the HRPT diffractometer at SINQ, PSI using wavelengths of 1.8852 and 1.4942 Å. Rietveld refinements were performed on the powder diffraction data using the GSAS suite of programs [18] using a pseudo-Voigt profile function. A correction for preferred orientation along the [0 0 1] direction was allowed in the refinement. Magnetic data were collected using a Quantum Design MPMS SQUID magnetometer in the temperature range 5–300 K. Zero-field-cooled (ZFC) and field-cooled (FC) data were collected on warming using an applied field of 0.5 T. The AC susceptibility was measured by varying the frequency from 30 Hz to 1 kHz with the field amplitude of 3 Oe. Electron diffraction (ED) and high resolution transmission electron microscopy (HRTEM) studies were performed on a JEOL 4000EX and a Phillips CM20 (ED) instrument. Samples for transmission electron microscopy were made by suspending the powder in ethanol and deposition onto a copper grid with a holey carbon layer. Calculated images for comparison with the experimental HRTEM images were made using the MacTempas software. X-ray absorption spectra at the Co K- and Mn K-edges were recorded in fluorescence mode at the European Synchrotron Radiation Facility ESRF in Grenoble, France on Beamline 25 at 298 K. The raw data were background subtracted and normalized using the program Athena [19]. The position of the Co- and Mn-edges was deduced from the most intense maximum of the first derivative of the corresponding X-ray absorption near-edge structure (XANES).

3. Results and discussion

3.1. Structural characterization

XRD showed the as-prepared materials to be single-phase and to crystallize in the tetragonal $I4/mmm$ space group with a structure related to that of $Sr_3Ti_2O_7$ [20] (Fig. 1a). No evidence of oxygen nonstoichiometry could be obtained from the XRD structural refinements and the oxide ion sites were therefore fixed at full occupancy corresponding to the stoichiometries $LaSr_2CoMnO_7$ and $La_{1.2}Sr_{1.8}CoMnO_7$. The reduction behaviour of these materials was followed by thermogravimetric measurements in which the materials were heated in flowing 10% H_2/N_2 (Fig. 2). The measurements suggest that the materials are reduced in two steps. The initial step ($T \approx 550$–750 °C) corresponds to loss of oxygen with retention of phase structure and crystal symmetry (as indicated by XRD), and the second step ($T > 800$ °C) corresponds to

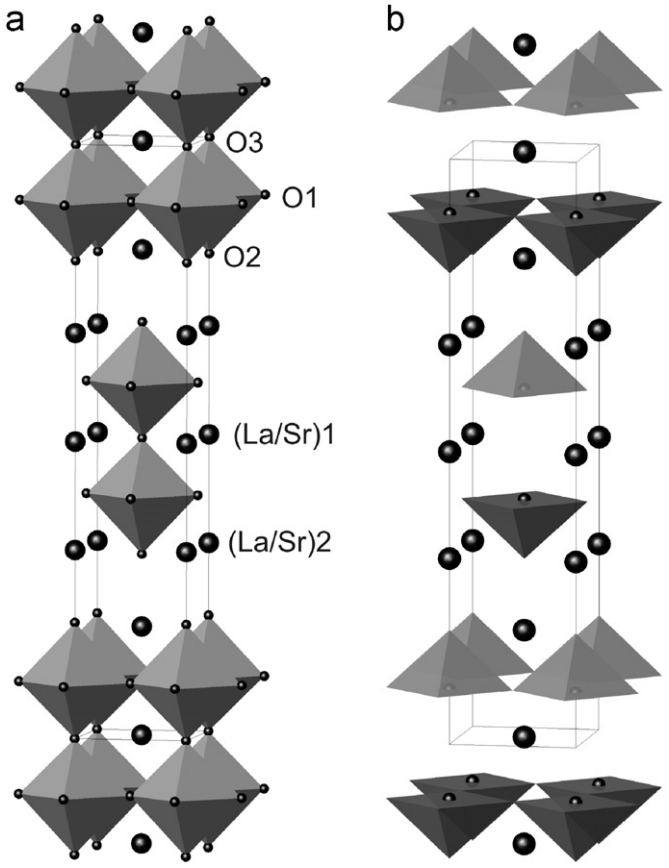

Fig. 1. (a) The $A_3B_2O_7$ $n=2$ RP structure showing BO_6 octahedra; (b) the reduced $A_3B_2O_6$ phase with apical oxygen vacancies giving BO_5 square pyramids.

partial decomposition to a $n=1$ RP phase and other decomposition products. The TG data suggest the first stage reduction products to be $LaSr_2CoMnO_6$ and $La_{1.2}Sr_{1.8}CoMnO_6$ (assuming the as-prepared materials to be $LaSr_2CoMnO_7$ and $La_{1.2}Sr_{1.8}CoMnO_7$). These reduced phases were prepared on a larger scale by heating the as-prepared materials in 10%H_2/N_2 at 700 °C for 12 h. The reduced phases have shown good stability in air at ambient temperature with no evidence of reoxidation.

The ED data recorded from the two reduced samples were identical. The data from one material ($LaSr_2CoMnO_6$) are given in Fig. 3. The ED data from the reduced materials can be indexed using cell parameters of approximately $a \approx 3.9$ Å and $c \approx 20.0$ Å and show the reflection condition hkl: $h+k+l=2n$. The very fine spots that are present on the [0 0 1] ED patterns at $h00$: $h=2n+1$ and $0k0$: $k=2n+1$ are due to the intersection of this pattern with weak streaks along the c^*-axis at these positions. The streaks were present on only some of the [uv0] ED patterns and are thought to relate to local differences in c-parameter (also observed on the HREM images) that probably reflect local changes in the oxygen vacancy order (*vide infra*). The cell parameters and the reflection condition are consistent with the $n=2$ RP type structure ($I4/mmm$ space group). The patterns clearly show that there is no superstructure. Fig. 4 shows a HRTEM image of the [1 0 0] zone of $LaSr_2CoMnO_6$. The HREM study confirmed the absence of long range oxygen-vacancy order in these materials. On this image the projected atom columns correspond to the black dots. The block with zigzag contrast is the rock salt type block. The outline of one unit cell is indicated by a black rectangle.

Representative NPD data (collected from $La_{1.2}Sr_{1.8}CoMnO_7$ and $La_{1.2}Sr_{1.8}CoMnO_6$ at room temperature) are shown in Fig. 5. Structural results are collected in Tables 1 and 2. Rietveld profile

refinements were performed using the ideal *I*4/*mmm* space group and the structural parameters of $Sr_3Ti_2O_7$ as a starting model. No evidence of oxygen nonstoichiometry could be observed in the as-prepared materials and the materials are therefore stoichiometric in oxygen, i.e. $LaSr_2CoMnO_7$ and $La_{1.2}Sr_{1.8}CoMnO_7$. The results are consistent with the thermogravimetric analysis which shows the as-prepared and oxygen-deficient materials as $LaSr_2CoMnO_7$, $La_{1.2}Sr_{1.8}CoMnO_7$ and $LaSr_2CoMnO_6$, $La_{1.2}Sr_{1.8}CoMnO_6$, respectively. In the final refinements for the reduced materials, correlation between thermal factors and site occupancies were minimised by using the chemical analysis to constrain the total oxygen composition at six per formula unit. On this basis, the refinements indicated that the oxygen vacancies were primarily located in the O3 sites (Fig. 1) with a slight deficiency in the O2 sites. The O1 site was fully occupied and was fixed for the final refinements. For $La_{1.2}Sr_{1.8}CoMnO_6$, additional constraints were necessary to aid convergence: the isotropic thermal factors for all oxygen sites were constrained to be equal, and U_{iso} for the Co/Mn site was held at a sensible value of 0.01 Å^2 to avoid slightly negative values. The refined structural parameters are given in Table 1. Unlike the situation in $Sr_3Mn_2O_6$ [15], oxide ion vacancies in $LaSr_2CoMnO_6$ and $La_{1.2}Sr_{1.8}CoMnO_6$ are mainly located in the apical O3 sites with no evidence of symmetry lowering due to vacancy order. The result is therefore consistent with the ED results. The *c* unit cell parameter will critically depend on the site occupancy of the common apical O3 site, and local occupancy variations could account for the streaking observed in a few ED patterns. The calculated HRTEM image using the refined model from NPD is shown as an inset to Fig. 4 (white border) and shows an excellent agreement with the experimental image at focus value $f = -100$ Å and thickness $t = 50$ Å. The vacancy distribution in $LaSr_2CoMnO_6$ and $La_{1.2}Sr_{1.8}CoMnO_6$ is consistent with that found in the O6 phases containing cobalt and iron [1,2] and

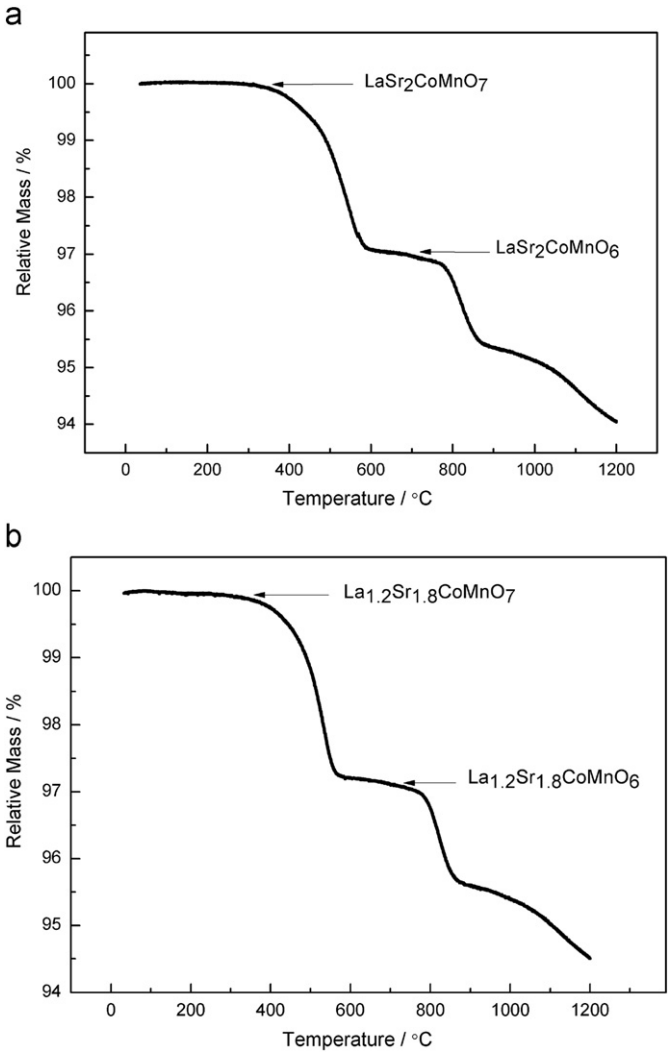

Fig. 2. Thermogravimetric analysis for the reduction of (a) $LaSr_2CoMnO_7$, (b) $La_{1.2}Sr_{1.8}CoMnO_7$ using 10% H_2 in N_2.

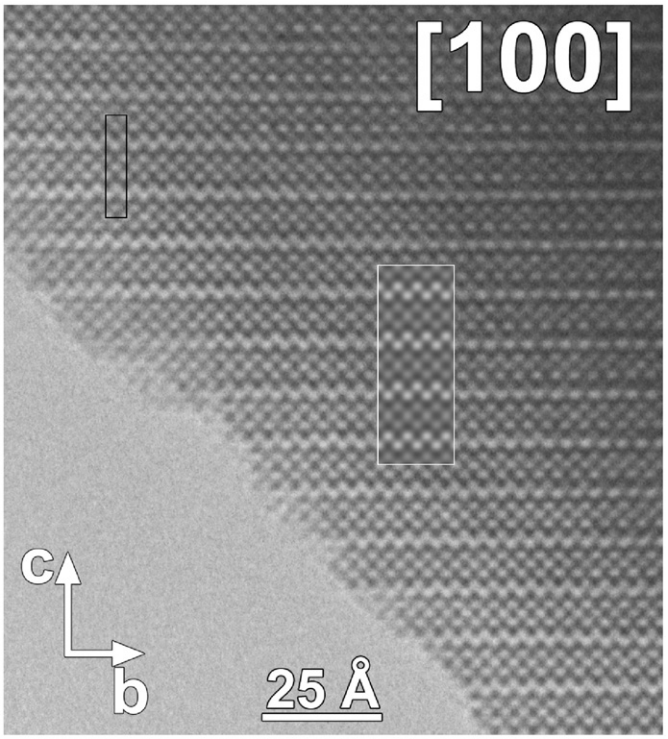

Fig. 4. HRTEM image along [1 0 0] of $LaSr_2CoMnO_6$.

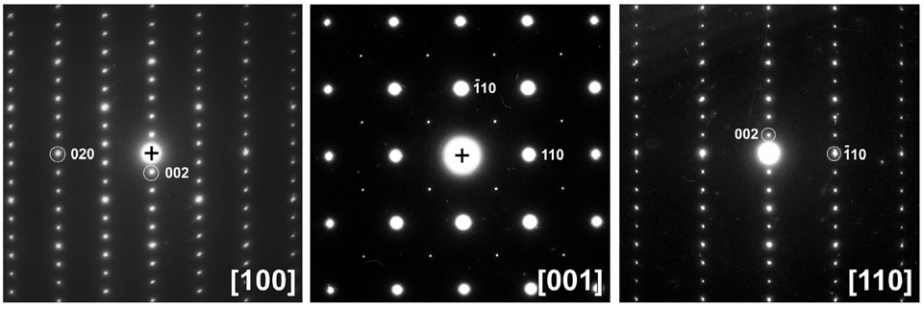

Fig. 3. ED data recorded along the main zone axes of $LaSr_2CoMnO_6$.

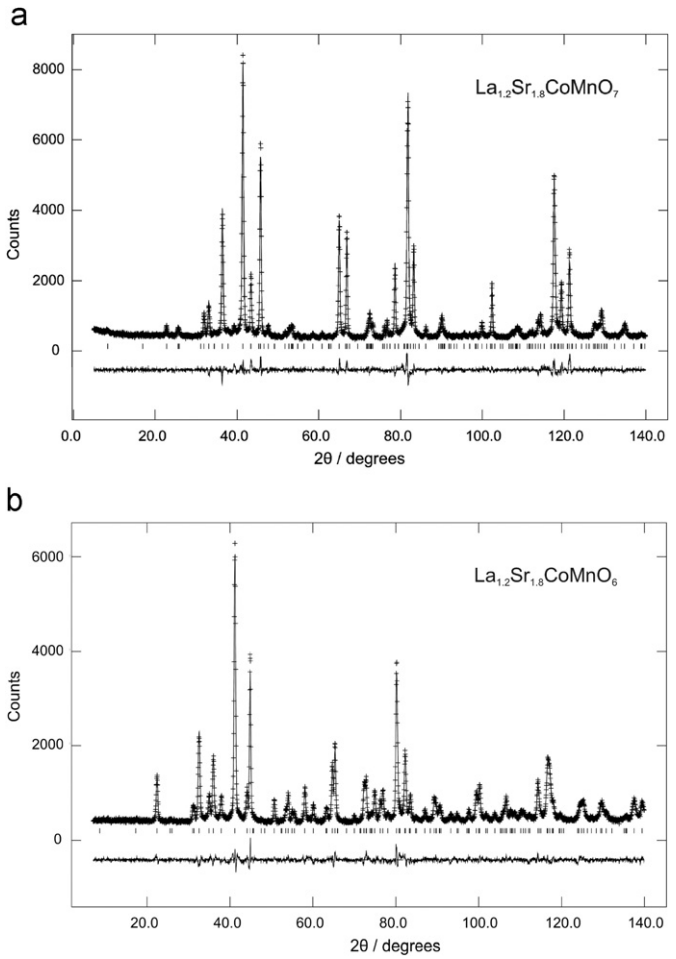

Fig. 5. Observed, calculated and difference profiles for NPD data collected from (a) $La_{1.2}Sr_{1.8}CoMnO_7$, and (b) $La_{1.2}Sr_{1.8}CoMnO_6$, at room temperature.

suggests a square pyramidal coordination around cobalt and manganese ions (Fig. 1b). A square pyramidal coordination for cobalt and manganese has been observed in the oxygen-deficient perovskite $YBaCoMnO_5$ [21]. No evidence of cation order is observed in the NPD data of any sample. In contrast, cation order was observed in the NPD study of the double perovskite La_2CoMnO_6 [22].

The Co- and Mn–K-edge XANES recorded from $LaSr_2CoMnO_7$ and $LaSr_2CoMnO_6$ are shown in Fig. 6, and the edge positions are collected in Table 3. The difficulty in ascertaining an edge position for the Co_3O_4 standard should be noted. The Co K- and Mn K-edge positions of $LaSr_2CoMnO_7$ both appear at higher energy than those of $LaSr_2CoMnO_6$. By comparison with the edge positions of the reference materials (Table 3) it would appear that cobalt and manganese in $LaSr_2CoMnO_7$ are present as Co^{3+} and Mn^{4+} and in $LaSr_2CoMnO_{6.0}$ as Co^{2+} and Mn^{3+} (although the edge positions are at higher energy than those of the standards, particularly for manganese).

The oxygen stoichiometry suggests the B-site oxidation state $(Co/Mn)^{3+/4+}$ in $LaSr_2CoMnO_7$. In contrast to the B-site state $(Co/Mn)^{3+}$ in La_2CoMnO_6, the $(Co/Mn)^{3+/4+}$ state failed to give any evidence of cation order in the NPD or ED study of $LaSr_2CoMnO_7$. It has been reported that the B-site state $(Co/Mn)^{3+}$ exhibits order in the form of Co^{2+} and Mn^{4+} in La_2CoMnO_6. However, this order disappears in the single layered material $LaSrCo_{0.5}Mn_{0.5}O_4$ [23]. The two dimensional nature of $LaSr_2CoMnO_7$ and $La_{1.2}Sr_{1.8}CoMnO_7$ seems to inhibit a three-dimensional cation order in these materials. The XANES study therefore indicates that $LaSr_2CoMnO_7$ contains a mixture of Mn^{4+} and Co^{3+}. The O7 to O6 reduction in this material suggests that Mn^{4+} and Co^{3+} ions are reduced to Mn^{3+} and Co^{2+}, respectively. The formation of a mixture of Mn^{2+} and Co^{3+} is chemically unfavoured [21] and is inconsistent with the XANES data. The Co^{2+}/Mn^{3+} state has been suggested for $YBaCoMnO_5$ [21] and $La_{2-x}Sr_xCo_{0.5}Mn_{0.5}O_{4-\delta}$; [9,23]. $La_{1.2}Sr_{1.8}CoMnO_7$, on the other hand, contains a mixture of $Mn^{4+}/Co^{3+}(Co^{2+})$ or $Mn^{4+}(Mn^{3+})/Co^{3+}$. The reduction to the O6-type phase $La_{1.2}Sr_{1.8}CoMnO_6$ suggests the formation of Co^{2+}/Mn^{3+} and some Mn^{2+} in this material. The

Table 1
Structural results for the refinement of the NPD data collected from different samples at room temperature.

Atom	x	y	z	$100 \times U_{iso}$ (Å^2)	Occupancy	Site symmetry
$LaSr_2CoMnO_7$, $a=3.82785(5)$ Å; $c=20.1265(4)$ Å; $wRp=0.0614$; $Rp=0.0475$; $\chi^2=1.809$						
(La/Sr)1	0	0	0.5	0.72(9)	0.333/0.667	2b
(La/Sr)2	0	0	0.3176(1)	0.71(6)	0.333/0.667	4e
Co/Mn	0	0	0.092(1)	1.5(6)	0.5/0.5	4e
O1	0	0.5	0.0949(1)	0.73(5)	1	8g
O2	0	0	0.1956(1)	1.10(9)	1	4e
O3	0	0	0	0.8(1)	1	2a
$La_{1.2}Sr_{1.8}CoMnO_7$, $a=3.83263(5)$ Å; $c=20.1618(4)$ Å; $wRp=0.0593$; $Rp=0.0466$; $\chi^2=2.441$						
(La/Sr)1	0	0	0.5	0.26(6)	0.4/0.6	2b
(La/Sr)2	0	0	0.3171(1)	0.43(4)	0.4/0.6	4e
Co/Mn	0	0	0.093(1)	0.5(3)	0.5/0.5	4e
O1	0	0.5	0.0952(1)	0.66(3)	1	8g
O2	0	0	0.1950(1)	0.88(7)	1	4e
O3	0	0	0	0.85(9)	1	2a
$LaSr_2CoMnO_6$, $a=3.8949(2)$ Å; $c=20.043(1)$ Å; $wRp=0.0518$; $Rp=0.0407$; $\chi^2=1.511$						
(La/Sr)1	0	0	0.5	1.12(8)	0.333/0.667	2b
(La/Sr)2	0	0	0.31826(9)	1.08(7)	0.333/0.667	4e
Co/Mn	0	0	0.089(1)	0.5(4)	0.5/0.5	4e
O1	0	0.5	0.0841(1)	2.39(6)	1	8g
O2	0	0	0.1987(1)	2.0(1)	0.925(6)	4e
O3	0	0	0	3(1)	0.15(1)	2a
$La_{1.2}Sr_{1.8}CoMnO_6$, $a=3.9160(2)$ Å; $c=19.915(1)$ Å; $wRp=0.0598$; $Rp=0.0468$; $\chi^2=2.204$						
(La/Sr)1	0	0	0.5	0.25(6)	0.4/0.6	2b
(La/Sr)2	0	0	0.31940(8)	0.82(5)	0.4/0.6	4e
Co/Mn	0	0	0.090(1)	1.00[a]	0.5/0.5	4e
O1	0	0.5	0.08299(9)	1.72(5)[b]	1	8g
O2	0	0	0.1995(1)	1.72(5)[b]	0.934(4)	4e
O3	0	0	0	1.72(5)[b]	0.132(8)	2a

[a] U_{iso} constrained.
[b] U_{iso} constrained equal.

Table 2
Selected bond lengths (Å) for the refined phases.

Bond	$LaSr_2CoMnO_7$	$La_{1.2}Sr_{1.8}CoMnO_7$	$LaSr_2CoMnO_6$	$La_{1.2}Sr_{1.8}CoMnO_6$
Co/Mn–O1	1.915(1)	1.9169(6)	1.950(1)	1.963(2)
Co/Mn–O2	2.10(3)	2.06(3)	2.20(2)	2.19(3)
Co/Mn–O3	1.84(3)	1.87(3)	1.79(3)	1.79(3)
(La/Sr)1–O1	2.704(1)	2.712(1)	2.575(1)	2.562(1)
(La/Sr)1–O3	2.70670(3)	2.71008(4)	2.7541(2)	2.7690(1)

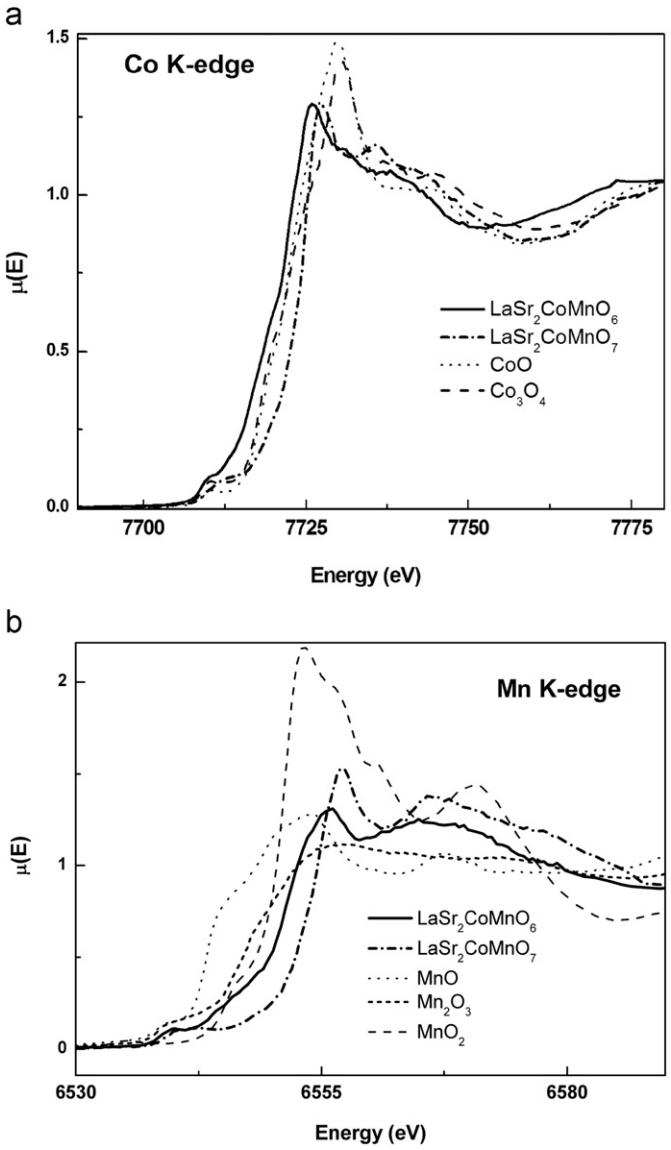

Fig. 6. XANES recorded from $LaSr_2CoMnO_7$ and $LaSr_2CoMnO_6$: (a) Co K-edge and (b) Mn K-edge.

formation of Mn^{2+} is also observed under the reduction of the single-layered material $La_{0.8}Sr_{1.2}Co_{0.5}Mn_{0.5}O_{4-\delta}$; [9].

The predominant reduction of Mn^{4+} and Co^{3+} to Mn^{3+} and Co^{2+} to form the O6-type materials suggests an expansion in the M–O bonds. The NPD data show a general expansion of M–O1 and M–O2 bonds while the M–O3 bonds undergo significant contraction (Table 2). However, it should be noted that the O3 site has an occupancy of only ~14% (Table 1) such that the M–O3 distance mainly reflects half the separation between M sites when the O3 site is empty. The true M–O3 distance is therefore uncertain. The reduction process was associated with an expansion in the *a* parameter and a contraction in the *c* parameter (e.g. $La_{1.2}Sr_{1.8}CoMnO_7$: $a=3.83263(5)$ Å, $c=20.1618(4)$ Å; $La_{1.2}Sr_{1.8}CoMnO_6$: $a=3.9160(2)$ Å; $c=19.915(1)$ Å). Similar effects have been observed for the reduction of $Sr_3Fe_2O_7$ to $Sr_3Fe_2O_6$ [1]. This can be related to the coordination requirements of (La/Sr)1. Under reduction, a contraction in (La/Sr)1 coordination sphere (achieved in the *z* direction, i.e. *c*) occurs due to removal of in-plane oxygen atoms (O3) and reduction of the coordination number from 12 to ~8. The apical contraction of the (La/Sr)1 coordination sphere can be observed through the significant reduction of (La/Sr)1–O1 bond lengths (from 2.704(1) Å to 2.575(1) Å, for example, in $LaSr_2CoMnO_7/LaSr_2CoMnO_6$).

Table 3
X-ray absorption edge positions recorded from the X-ray absorption near-edge structure.

Compound	Co K-edge position (±0.2)(eV)	Mn K-edge position (±0.2)(eV)
CoO	7721.5	–
Co_3O_4	7722.0[a]	–
MnO	–	6543.4
Mn_2O_3	–	6547.2
MnO_2	–	6551.5
$LaSr_2CoMnO_7$	7724.3	6554.3
$LaSr_2CoMnO_6$	7721.5	6550.4

[a] Plus two other maxima of almost equal intensity at 7718.2 and 7728.3 eV.

3.2. Magnetic susceptibility

Fig. 7 shows the temperature dependence of the magnetic susceptibilities of $LaSr_2CoMnO_7$ and $La_{1.2}Sr_{1.8}CoMnO_7$ in the temperature range 5–300 K. Plots of the reciprocal of the molar susceptibility against temperature for these materials (insets in Fig. 7) suggest a non Curie–Weiss behaviour. However, the plots display a decreased gradient on cooling which suggests the predominance of ferromagnetic (FM) interactions. The data for $LaSr_2CoMnO_7$ are very similar to those previously reported for this material synthesized using ceramic methods [17], and confirm the complex nature of the magnetic interactions at low temperature. The application of the Curie–Weiss law to the high temperature magnetic susceptibility data gives positive values of θ which is consistent with FM interactions. Above 200 K, the θ values are 33.1 and 46.2 K for $LaSr_2CoMnO_7$ and $La_{1.2}Sr_{1.8}CoMnO_7$, and the effective moments are 6.21 and 6.50 μ_B, respectively. The relatively high effective moments suggest a high spin state of Co^{3+} in these materials; the effective moments are in very good agreement with the theoretical spin-only values for high-spin Mn^{4+}/Mn^{3+} and Co^{3+} ions (6.24 and 6.39 μ_B for $LaSr_2CoMnO_7$ and $La_{1.2}Sr_{1.8}CoMnO_7$, respectively). The magnetic behaviour of the two oxidised phases is seen to show subtle differences. $LaSr_2CoMnO_7$ shows what appears to be a fairly conventional antiferromagnetic (AFM) transition at ~70 K, but a distinct divergence of field-cooled (FC) and zero-field-cooled (ZFC) susceptibilities occurs below ~60 K.

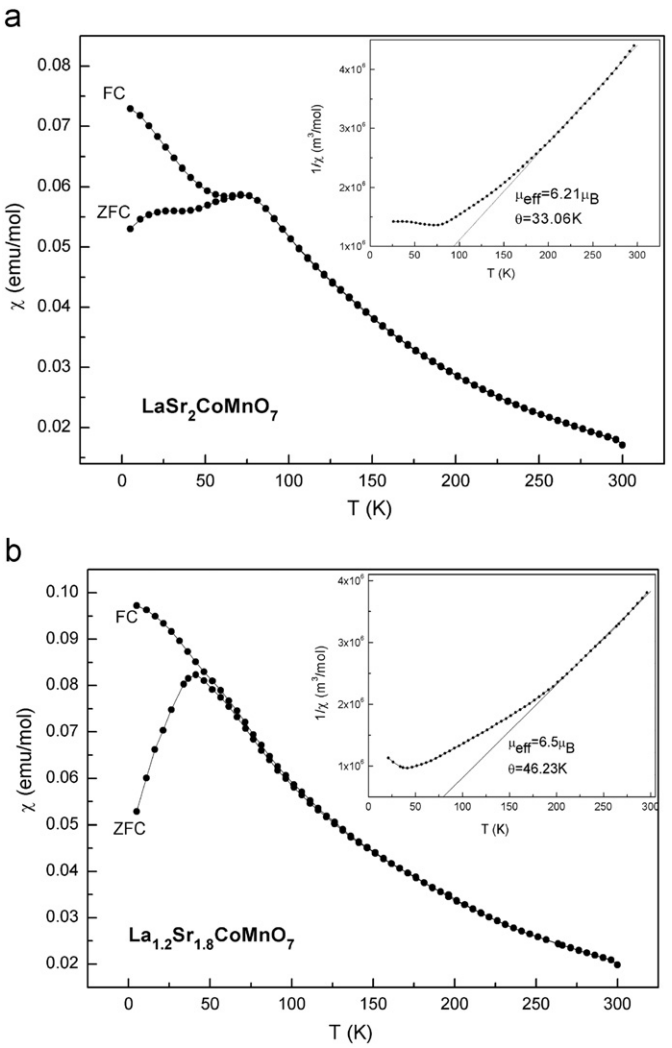

Fig. 7. Variation of magnetic susceptibility (ZFC and FC) and the inverse magnetic susceptibilities (ZFC) with temperature for (a) $LaSr_2CoMnO_7$ and (b) $La_{1.2}Sr_{1.8}CoMnO_7$.

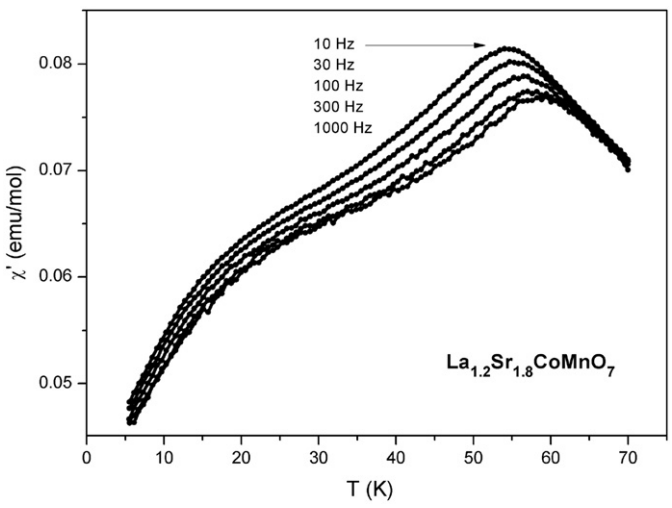

Fig. 8. AC susceptibility data recorded from $La_{1.2}Sr_{1.8}CoMnO_7$.

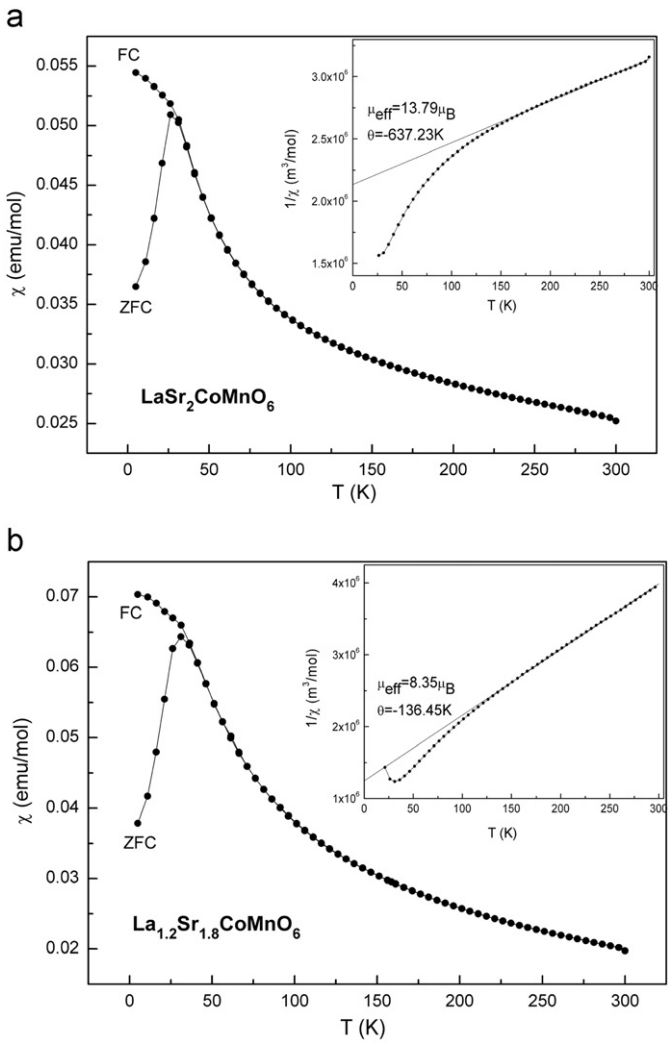

Fig. 9. Variation of magnetic susceptibility (ZFC and FC) and the inverse magnetic susceptibilities (ZFC) with temperature for (a) $LaSr_2CoMnO_6$ and (b) $La_{1.2}Sr_{1.8}CoMnO_6$.

This is suggestive of re-entrant spin glass behaviour (see, for example, [23]). $La_{1.2}Sr_{1.8}CoMnO_7$ shows a regular spin glass transition with a freezing temperature of ~50 K. The spin glass state can be attributed to competitive ferromagnetic (FM) and antiferromagnetic (AFM) interactions between disordered Mn^{4+} and Co^{3+} ions: Mn–Mn and Co–Co interactions would be expected to be AFM whereas Mn–Co exchange should be FM. The change in behaviour between $LaSr_2CoMnO_7$ and $La_{1.2}Sr_{1.8}CoMnO_7$ can be attributed to the enhanced frustration introduced by the presence of Mn^{3+} in addition to Mn^{4+} cations. The second cusp observed at lower temperature (~25 K) for $LaSr_2CoMnO_7$ can be related to a possible change in the spin state of Co^{3+} (to low or intermediate spin) [17]; under the applied conditions no obvious effect is seen, for $La_{1.2}Sr_{1.8}CoMnO_7$. The spin glass behaviour in these materials has been confirmed by AC magnetic susceptibility measurements. The frequency dependence of the AC magnetic susceptibility of $La_{1.2}Sr_{1.8}CoMnO_7$, Fig. 8, shows that the location of the cusp at the freezing temperature is dependent on the frequency of the AC susceptibility measurement, which is a characteristic feature of spin glasses. Interestingly, the low temperature cusp is observed in this material under these conditions.

The reduced materials $LaSr_2CoMnO_6$ and $La_{1.2}Sr_{1.8}CoMnO_6$ also show spin glass behaviour at low temperatures (Fig. 9). This can be attributed to competitive FM and AFM interactions between high spin Mn^{3+} and Co^{2+} ions. In contrast to the oxidised samples, the inverse susceptibility plots (see insets in Fig. 9) show that the magnetic interactions are now predominately AFM in nature. This

is consistent with the magnetic behaviour of Mn^{3+} and Co^{2+} in related $n=1$ RP phases [24]. Above 200 K, the θ values are -637.2 and -136.5 for $LaSr_2CoMnO_6$ and $La_{1.2}Sr_{1.8}CoMnO_6$ and the effective moments are 13.79 and 8.35 μ_B, respectively. The significantly high effective moments (compared with the spin-only values, 6.25 and 6.42 μ_B per formula unit, respectively) suggest the presence of FM clusters of Co^{2+} and Mn^{3+} ions in these materials. Similar clusters have previously been observed in Co-doped $LaSr_2CoMnO_7$ [25] and the single-layered material $La_{1.2}Sr_{0.8}MnO_{4.27}$ [26].

4. Conclusions

The $n=2$ Ruddlesden–Popper phases $LaSr_2CoMnO_7$ and $La_{1.2}Sr_{1.8}CoMnO_7$ have been synthesized by a sol–gel method. The materials crystallize in the tetragonal *I4/mmm* space group with no evidence of long-range cation order. The materials have been reduced under hydrogen to form the O6-type phases $LaSr_2CoMnO_6$ and $La_{1.2}Sr_{1.8}CoMnO_6$. In these materials, the crystal symmetry is retained (*I4/mmm* space group) and oxygen is removed mainly from the apical sites which link the MO_6 octahedra perpendicular to the perovskite layers; this provides a square pyramidal coordination for the cobalt and manganese ions. The oxidation states Co^{3+}/Mn^{4+} and Co^{2+}/Mn^{3+} predominate in the as-prepared and reduced materials, respectively. The materials are spin glasses at low temperature with the dominant magnetic interactions changing from ferro- to antiferromagnetic following O7–O6 reduction.

Acknowledgments

We thank the Egyptian Education Bureau (London) for financial support (H. El Shinawi). We are also grateful to V. Pomjakushin for assistance with the collection of NPD data. We acknowledge the European Synchrotron Radiation Facility and thank Dr. G. Castro for assistance in using Beamline 25. We thank The Spanish Ministry of Science and Innovation for travel grants (JFM,TH,BS). J. Hadermann and A. Bertha acknowledge financial support from the European Union under the Framwork 6 progrm under a contract for an Integrated Infrastructure Initiative, reference 026019 ESTEEM.

References

[1] S.E. Dann, M.T. Weller, D.B. Currie, J. Solid State Chem. 97 (1992) 179.
[2] S.E. Dann, M.T. Weller, J. Solid State Chem. 115 (1995) 499.
[3] J.M. Hill, B. Dabrowski, J.F. Mitchell, J.D. Jorgensen, Phys. Rev. B 74 (2006) 174417.
[4] L. Viciu, H.W. Zandbergen, Q. Xu, Q. Huang, M. Lee, R.J. Cava, J. Solid State Chem. 179 (2006) 500.
[5] Y. Bréard, C. Michel, M. Hervieu, F. Studer, A. Maignan, B.B. Raveau, Chem. Mater. 14 (2002) 3128.
[6] M. Crespin, J.M. Bassat, P. Odier, P. Mouron, J. Choisnet, J. Solid State Chem. 84 (1990) 165.
[7] M. Crespin, C. Landron, P. Odier, J.M. Bassat, P. Mouron, J. Choisnet, J. Solid State Chem. 100 (1992) 281.
[8] H. El Shinawi, C. Greaves, J. Solid State Chem. 181 (2008) 2705–2712.
[9] H. El Shinawi, J.F. Marco, F.J. Berry, C. Greaves, J. Solid State Chem. 182 (2009) 2261.
[10] A. Bowman, M. Allix, D. Pelloquin, M.J. Rosseinsky, J. Am. Chem. Soc. 128 (2006) 12606.
[11] H. Kageyama, T. Watanabe, Y. Tsujimoto, A. Kitada, Y. Sumida, K. Kanamori, K. Yoshimura, N. Hayashi, S. Muranaka, M. Takano, M. Ceretti, W. Paulus, C. Ritter, G. André, Angew. Chem. Int. Ed. 47 (2008) 5740.
[12] M.E. Leonowicz, K.R. Poeppelmeier, J.M. Longo, J. Solid State Chem. 59 (1985) 71.
[13] M.A. Hayward, M.J. Rosseinsky, Chem. Mater. 12 (2000) 2182–2195.
[14] J.F. Mitchell, J.E. Millburn, M. Medarde, S. Short, J.D. Jorgensen, J. Solid State Chem. 141 (1998) 599.
[15] L.J. Gillie, A.J. Wright, J. Hadermann, G. Van Tendeloo, C. Greaves, J. Solid State Chem. 175 (2003) 188.
[16] N. Nguyen, L. Er-Rakho, C. Michel, J. Choisnet, B. Raveau, Mater. Res. Bull. 15 (1980) 891.
[17] T.I. Chupakhina, G.V. Bazuev, Russ. J. Inorg. Chem. 53 (2008) 681.
[18] A.C. Larson, R.B. Von Dreele, General Structural Analysis System, Los Alamos National Laboratory, Los Alamos, NM, 1994.
[19] B. Ravel, M. Newville, J. Synchrotron Rad. 12 (2005) 537.
[20] S.R. Ruddlesden, P. Popper, Acta Crystallogr. 10 (1957) 538;
S.R. Ruddlesden, P. Popper, Acta Crystallogr. 11 (1958) 54.
[21] P. Karen, E. Suard, F. Fauth, P.M. Woodward, Solid State Sci. 6 (2004) 1195.
[22] C.L. Bull, D. Gleeson, K.S. Knight, J. Phys.: Condens. Matter 15 (2003) 4927.
[23] S.M. Rao, M.K. Wu, J.K. Srivatava, B.H. Mok, C.Y. Lu, Y.C. Liao, Y.Y. Hsu, Y.S. Hsiue, Y.Y. Chen, S. Neeleshwar, S. Tsai, J.C. Ho, H.L. Liu, Phys. Lett. A 324 (2004) 71.
[24] H. El Shinawi, C. Greaves, Z. Anorg. Allg. Chem. 635 (2009) 1856.
[25] R.L. Zhang, W.H. Song, Y.Q. Ma, J. Yang, B.C. Zhao, Z.G. Sheng, J.M. Dai, Y.P. Sun, Phys. Rev. B 70 (2004) 224418.
[26] R.K. Li, C. Greaves, J. Solid State Chem. 153 (2000) 34.